Enhanced p-Type Conductivity of ZnTe Nanoribbons by Nitrogen Doping

Shanying Li,[†,‡] Yang Jiang,*[,†] Di Wu,[†] Li Wang,[§] Honghai Zhong,[†] Bo Wu,[†] Xinzheng Lan,[†] Yongqiang Yu,[§] Zhuangbing Wang,[§] and Jiansheng Jie*[,§]

School of Materials Science and Engineering and School of Electronic Science and Applied Physics, Hefei University of Technology, Hefei, Anhui 230009, People's Republic of China, and Department of Chemical Engineering, Henan University of Urban Construction, Pingdingshan, Henan 467044, People's Republic of China

Single-crystalline intrinsic and N-doped p-type ZnTe nanoribbons (NRs) were synthesized via the thermal evaporation method in argon-mixed hydrogen and nitrogen-mixed ammonia, respectively. Both intrinsic and doped ZnTe nanoribbons had zinc blende structure and uniform geometry. X-ray diffraction peaks of N-doped ZnTe nanoribbons had an obvious shift toward higher angle direction as compared with intrinsic ZnTe. X-ray photoelectron spectroscopy detection confirmed that the dopant content of nitrogen in ZnTe nanoribbons was close to 1%. Field-effect transistors based on both intrinsic and N-doped ZnTe nanoribbons were constructed. Electrical measurements demonstrated that N-doping led to a substantial enhancement in p-type conductivity of ZnTe nanoribbons with a high hole mobility of 1.2 cm^{-2} V^{-1} S^{-1} and a low resistivity of 0.14 Ω cm in contrast to the 6.2×10^{-3} cm^{-2} V^{-1} S^{-1} and 45.1 Ω cm for intrinsic nanoribbons. Moreover, the defect reaction mechanism was proposed to explain the p-type behaviors of both the intrinsic and the N-doped ZnTe nanoribbons. The ZnTe nanoribbons with enhanced p-type conductivity may have important potential applications in nanoelectronic and optoelectronic devices.

Introduction

As direct wide band gap semiconductors, II–VI group compounds present a wide range of electrical and optical properties making them an important class of materials in electronic, optoelectronic, display, and energy conversion applications. Recently, semiconductor nanostructures with high-aspect ratio, such as nanowires (NWs), nanoribbons (NRs), nanotubes (NTs), or multibranched structures, have attracted considerable attention because of the interesting physical and chemical properties that appeared in nanoscale.[1–7] To realize the practical applications of semiconductor nanostructures in nanodevices, doping is an essential issue that must be addressed to achieve the rational control of their electrical and photoelectrical properties. However, most II–VI nanostructures show n-type conductivity and p-type doping that is hard to realize because of the strong self-compensation effects.[1,8–12] Thus far, initial studies on the p-type doping of ZnO,[13–15] ZnS,[16] and ZnSe[17] NWs/NRs have been reported representing an exciting progress toward II–VI nanodevices. Nevertheless, the p-type doping remains a large challenge, and more experiments are needed to further develop the p-type conductivity of II–VI nanostructures in terms of doping efficiency, reliability, and reproducibility.

ZnTe is an important II–VI group semiconductor material and has a direct band gap of 2.26 eV at room temperature.[18] The applications of ZnTe in green light emitting diodes, X-ray detectors, and solar cells have been well recognized.[19–23] Interestingly, the intrinsic ZnTe usually exhibits p-type conductivity, and this character can be further enhanced by appropriate doping allowing the formation of p–n junctions as well as superlattice structures by combining ZnTe with other n-type semiconductors.[22,24,25] To date, several wet-chemistry methods have been used to synthesize ZnTe nanostructures. Zhang et al. reported the synthesis of ZnTe NRs in organic solutions.[19,26,27] Li et al. reported the synthesis of ZnTe NWs arrays by using a pulsed electrochemical deposition method in aqueous solution.[26] Yong et al. also reported the formation of ZnTe NWs by oriented attachment in organic solution.[27] Nevertheless, ZnTe nanostructures formed by these wet-chemistry methods usually have small length and ratio of length to radius and low crystal quality because of the residual solvent, which makes device fabrication difficult.[28] Recently, Huo et al. reported that the p-type conductivity of ZnTe nanowires could be enhanced by dealing the intrinsic ZnTe NWs with $Cu(NO_3)$ solution.[29] However, the postgrowth doping method is complicated and difficult to control compared with the usual in situ doping particularly in the case of advanced device structures such as p–n junction that are needed to be fabricated. A simple method with high-doping efficiency is much desired to realize ZnTe nanostructures with well-controlled p-type conductivity.

Herein, we report a new method that involves the use of gaseous NH_3 dopant source in the vapor–liquid–solid (VLS) growth of ZnTe NRs. The p-type conductivity of the ZnTe NRs was significantly improved because of the incorporation of N acceptors. The in situ doping method with gaseous dopant is advantageous over other methods, in which solid dopant or postgrowth doping is adopted, on the basis of controllability and effectiveness.[15,16,30–33]

Experimental Details

Growths of ZnTe NRs were carried out in an alumina tube furnace via thermal evaporation. High-purity ZnTe powder (99.999%) was loaded into an alumina boat and was placed at

* Authors to whom correspondence should be addressed. E-mail: apjiang@hfut.edu.cn (Y.J.) and jsjie@hfut.edu.cn (J.J.).
† School of Materials Science and Engineering, Hefei University of Technology.
‡ Henan University of Urban Construction.
§ School of Electronic Science and Applied Physics, Hefei University of Technology.

Enhanced p-Type Conductivity of ZnTe Nanoribbons

J. Phys. Chem. C, Vol. 114, No. 17, 2010 **7981**
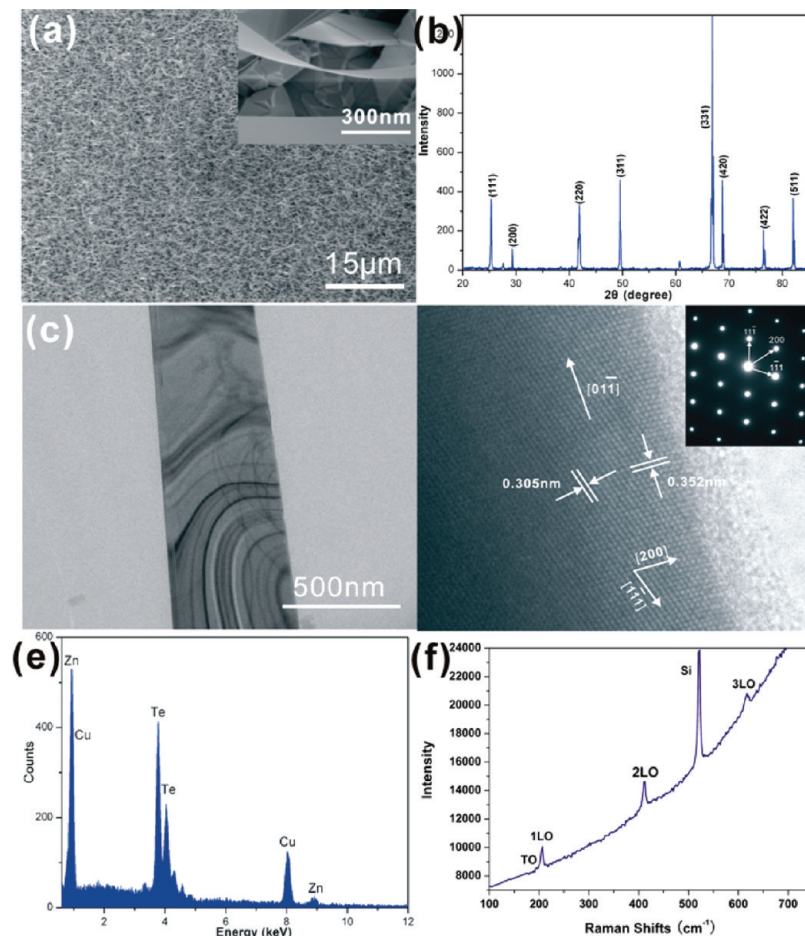
Figure 1. (a) SEM images of the typical as-prepared p-type ZnTe nanoribbons. (b) XRD patterns of ZnTe nanoribbons. (c) A TEM bright-field image of ZnTe nanoribbon. (d) An HRTEM image of ZnTe nanoribbon. The inset is the SAED pattern of ZnTe nanoribbon. (e) An EDS spectrum of ZnTe nanoribbons. (f) Raman spectrum of ZnTe nanoribbons at room temperature.

the center of the tube furnace, and Si substrates coated with a layer of 5 nm gold catalyst were placed in the downstream direction 10 cm from the source. The tube was then evacuated to a base pressure of 10^{-2} Torr. For the synthesis of intrinsic ZnTe NRs, a mixture of Ar and H_2 gases (10%) was used as the carrier gas and was kept at a constant flow rate of 50 standard cubic centimeters per minute (sccm), while instead, ammonia and nitrogen mixture was adopted for N-doped ZnTe NRs. The percent of NH_3 in the total carrier gas was varied to control the doping concentration. During the experiments, the ZnTe source and the substrates were heated at a rate of 10 K min^{-1} to 1130 and 890 K, respectively. Pressure for the reaction was maintained at 500 Torr, and the duration was 2 h.

Morphology and structure characterizations of the as-synthesized NRs were performed by using X-ray diffraction (XRD, D/max-γB), field-emission scanning electron microcopy (FESEM, SIRION 200, FEI), and high-resolution transmission electron microscopy (HRTEM, JEM-2010, JEOL) with selected-area electron diffraction (SAED). Compositions of the nano-ribbons were determined by energy-dispersive X-ray spectros-copy (EDS, OXFORD, attached on the TEM) and X-ray photoelectron spectroscopy (XPS, ESCALAB 250). The Raman spectra were excited with 514.5 nm argon-laser lines and were measured using confocal laser microRaman spectrometer (LA-BRAM-HR).

To assess the electrical transport properties of intrinsic and doped ZnTe NRs, field-effect transistors based on single NR were constructed. ZnTe NRs were first collected from the Si

substrates and were dispersed in ethanol. Then, the suspension was deposited on a degenerately doped p-type silicon wafer that was precovered with 30 nm high-k dielectric of hafnium oxide, which was deposited by atomic layer deposition (ALD Savan-nah-200). A mesh grid that consisted of 5 μm tungsten wire was used as the shadow mask, and nickel electrodes (100 nm) were deposited in a high-vacuum electron-beam evaporation system. The electrical measurements were conducted by using a semiconductor characterization system (Keithley 4200) at room temperature.

Results and Discussion

Figure 1a shows the SEM image of the as-synthesized intrinsic ZnTe (i-ZnTe) NRs in H_2/Ar (10%/90%) atmosphere. The NRs have a uniform ribbonlike geometry with width of 200$\sim$600 nm, thickness of $\sim$30 nm, and length of >20 μm. The XRD pattern is depicted in Figure 1b; all the diffraction peaks can be assigned to ZnTe with zinc blende structure (JCPDS No. 15$-$0746). From the typical TEM image of the ZnTe NR (Figure 1c), it could be seen that the surface of the NR is clear and smooth and that there are no particles and impurities on it revealing the good crystallinity and uniformity of the NR. Furthermore, Figure 1d shows the HRTEM image; the lattice spacings of 0.305 and 0.352 nm correspond to the (200) and (1$-$11) planes, respectively. The corresponding SAED pattern recorded along the [011] zone axis reveals that the ZnTe NRs are single crystalline with growth direction of [01$-$1]. The i-Zn: Te atomic ratio is estimated to be about 43:57, and the content
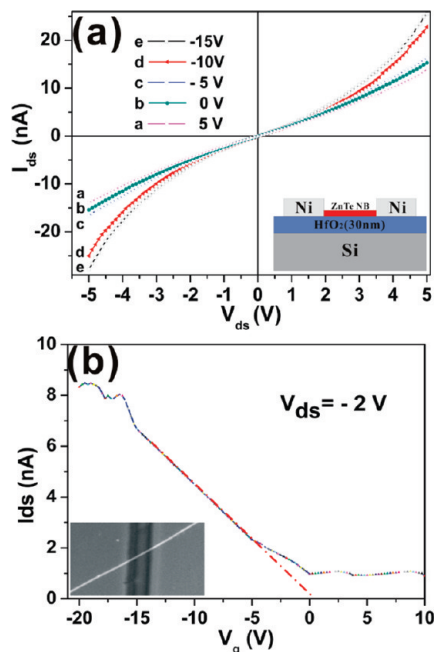
Figure 2. Electron-transfer characteristics of intrinsic ZnTe SNRFET in Ar–H$_2$ (90% + 10%) ambient. (a) I_{ds} vs V_{ds} curves for different V_g that range from 5 to (−15) V. The inset is a schematic diagram of ZnTe SNRFET. (b) I_{ds} vs V_g curve measured at $V_{ds} = -2$ V. The inset is the SEM image of a typical SNRFET device.

of Te is much higher than Zn from the EDS spectrum (Figure 1e) revealing a large nonstoichiometry of the product and implying that a large number of Zn vacancies ($\mathbf{V''_{Zn}}$) may exist in the NRs. Figure 1f depicts the Raman spectrum of the i-ZnTe nanoribbons. Scattering peaks located at 206, 412, and 619 cm^{-1} can be assigned to the ZnTe with LO, 2LO, and 3LO longitudinal optical phonon modes, respectively. Also, the peak at 177 cm^{-1} is the transverse optical phonon mode (TO). The results are in agreement with the previous reports for the Raman spectrum of i-ZnTe.[34,35]

Electrical transport characteristics of the ZnTe NRs were evaluated on the basis of the nano-FETs fabricated from single NR. The inset in Figure 2a illustrates the device structure of the field effect transistor (FET) in which the heavily doped Si substrate and the HfO$_2$ layer (30 nm) serve as the back-gate and the gate dielectric, respectively, whereas the SEM image for a typical device is shown in the inset of Figure 2b. From the source–drain current versus voltage (I_{ds}–V_{ds}) curves obtained at varied gate voltages (V_g) from +5 V to −15 V in a step of 5 V, we observe that the conductance of the NR monotonously increases with the decreasing of the V_g revealing a typical p-type semiconductor character. On the basis of the EDS analysis result, the p-type behavior of the i-ZnTe NRs is likely attributed to the intrinsic defects such as Zn vacancies in the NRs, which is consistent with the observations that the i-ZnTe should tend to exhibit p-type characteristics because of the self-compensation effect.[22,25] The resistance of i-ZnTe NRs (R_{i-ZnTe}) is estimated to be about 3.5 × 10^8 Ω and resistivity (ρ_{i-ZnTe}) is about 45.1 Ω cm by taking account the dimensions of the NR. Figure 2b depicts the I_{ds}–V_g curve at $V_{ds} = -2$ V. The hole mobility (μ_h) can be deduced on the basis of the equation $g_m = \mu_h(Z/L)C_0V_{ds}$,[8,29,36] where $g_m = dI_{ds}/dV_g$ is the transconductance in the linear region (V_g from −5 to −10 V) and the value is about 0.4 nS, Z/L is the ratio of channel width to channel length and is equal to 200/4600 for our configuration, and C_0 is the gate capacitance per unit of 737.5 nF/cm^2 for the HfO$_2$ dielectric with 30 nm thickness. C_0

for the HfO$_2$ layer is much larger than that for the SiO$_2$ dielectric layer (11.5 nF/cm^2 for 300 nm thickness SiO$_2$). Therefore, because of the high capacitance afforded by the high-k HfO$_2$ layer, the ZnTe NR FETs with HfO$_2$ dielectric can show better device performance in contrast to the weak gating effect for the duplicate on SiO$_2$/Si substrate.[37] This is the important reason why we use HfO$_2$ instead of conventional SiO$_2$ as the gate dielectric in device construction. On the basis of the above equation, μ_h is deduced to be about 6.2 × 10^{-3} cm^2 V^{-1} S^{-1}. This value is much lower than the ZnTe thin films of 540 cm^2 V^{-1} S^{-1}.[38] The hole concentration (n_h) thus can be estimated to be about 2.2 × 10^{19} cm^{-3} from the relationship of $\rho_{i-ZnTe} = 1/n_h e\mu_h$. By extrapolating the I_{ds}–V_g curve to the V_g axis, the threshold voltage (V_{th}) is estimated to be about 1.0 V.

The p-type character of the i-ZnTe NRs can be explained in terms of defect theory. For the compound semiconductors, each element constituting the compounds usually has different dissociation pressure and sublimating temperature thus leading to the deviation of the product from the stoichiometric composition during the sublimation and deposition processes. In our case, the content of Te in the ZnTe NRs tends to exceed that of Zn because the latter has a higher saturated vapor pressure.[22,39] The growth of i-ZnTe NRs in our work can be described as follows. At elevated temperatures, the ZnTe source powder will sublimate and meanwhile will react with H$_2$ in the carrier gas resulting in a complicated growth atmosphere consisting of Zn, Te, and H atomic clusters; ZnTe, H$_2$Te, and H$_2$ molecular clusters; and possibly some ionized groups. Compared with Te, Zn is much easier to volatilize and has higher vapor pressure. In this case, not all the decomposed Zn molecules will react with Te to form ZnTe at the NR growth region, which would give rise to the deviation from the stoichiometry. As a result, several Zn vacancies would be formed and would contribute to the p-type conductivity. In fact, for our experiments, a layer of Zn powder depositing on the inner surface of the tube was observed at the downstream position 15 cm from the ZnTe NR growth region and a temperature drop of about 200 K. Generally, the deviation from stoichiometry for the semiconductor compounds can be denoted as the component defect which can be expressed as a defect reaction equation as follows.

$$\frac{1}{2}\text{Te}_2(g) = \mathbf{V''_{Zn}}\text{Te}^{\times}_{\text{Te}} + 2h^{\bullet}$$
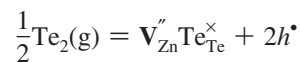
where Te$_2$(g) is gaseous molecule, $\mathbf{V''_{Zn}}$ is the Zn vacancy, Te$^{\times}_{\text{Te}}$ is the neutral Te, and $h^{\bullet}$ is one positively charged vacancy. Usually, the cations present as the bivalent Zn^{2+}. When Te ion is in excess, the partial cation will turn into quasi-trivalent (Zn^{2+} +$h^{\bullet}$) to maintain overall charge neutrality. The holes can be considered as one weakly bound hole by Zn^{2+}, and they can be readily released when subjected to thermal excitation, which will contribute to the p-type conductivity of i-ZnTe. On the other hand, taking into account the band structure, the acceptor energy levels will be formed by the neutral Zn vacancy of $\mathbf{V^{\times}_{Zn}}$ and the ionized Zn vacancy of $\mathbf{V''_{Zn}}$ in the forbidden energy gap. The ionized vacancies will generate holes at the top of the valence band and then will demonstrate p-type conductivity.

To enhance the p-type conductivity of the ZnTe NRs, the N-doped ZnTe (ZnTe:N) NRs were synthesized by using NH$_3$ as the gaseous dopant source. A series of samples were synthesized with different NH$_3$ concentrations up to 50%. Figure 3a and b depict the typical SEM and TEM images of ZnTe:N NRs with 10% NH$_3$ concentration doping. The shapes of doped ZnTe NRs are as uniform as the undoped ones, while their

Enhanced p-Type Conductivity of ZnTe Nanoribbons

J. Phys. Chem. C, Vol. 114, No. 17, 2010 **7983**
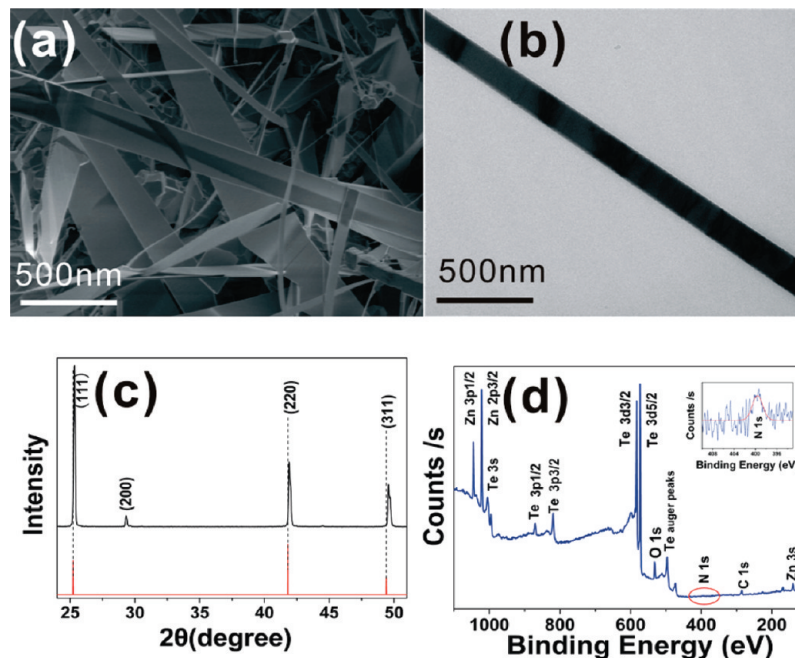
Figure 3. (a) SEM images of the typical as-prepared N-doped ZnTe nanoribbons. (b) A TEM bright-field image of ZnTe nanoribbon. (c) XRD patterns of N-doped ZnTe NRs. (d) XPS spectrum of N-doped ZnTe NRs. The inset is N XPS spectrum.

surfaces still stay clean and smooth. Because of the incorporation of N into the lattice, which has a smaller radius than Te, the shift of the diffraction peaks toward a higher angle is observed in the XRD pattern of the p-ZnTe NRs (Figure 3c). XPS detection performed on the ZnTe:N also confirms the existence of N in the NRs (Figure 3d). A weak peak at 398 eV corresponding to the N 1s core level was observed in addition to the strong Zn and Te signals[40,41] indicating that N is indeed incorporated into ZnTe:N NRs. Semiquantitative XPS analysis reveals that N concentration was close to 1%. However, the signal of N in XPS is very weak particularly for the sample with lower doping concentration; therefore, electrical measurements are desired to determine the impact of N doping on the p-type transport properties of ZnTe NRs.

FETs based on the individual ZnTe:N NRs are constructed to evaluate the p-type conductivity of ZnTe:N NRs. The method used for the construction of ZnTe:N NR FETs is the same with i-ZnTe NR FETs. Figure 4 shows the typical electrical transfer characteristics of a single ZnTe:N NR (10% NH_3). Significantly, the resistivity of the ZnTe:N NRs ($\rho_{ZnTe:N}$) has decreased to be 17.94 Ω cm, which fell by about two-thirds compared to that of i-ZnTe NRs. The device shows an obvious gating effect while V_g varies from 10 V to -15 V in a step of 5 V and I_{ds} increases monotonously with the decreasing of V_g revealing a typical p-type semiconductor character. Taking into account the width (Z) of ZnTe of 260 nm and the channel length (L) of 4600 nm, the channel transconductance ($g_m = dI_{ds}/dV_g$) is calculated to be 2.7 ns at $V_{ds} = -2$ V from the $I_{ds}-V_g$ curve (Figure 4b) leading to a hole mobility of about 4.2×10^{-2} cm^2 V^{-1} S^{-1}. Therefore, the hole concentration for the ZnTe:N NRs is estimated to be about 8.3×10^{18} cm^{-3}. Moreover, the threshold voltage (V_{th}) of the NR FET is deduced to be 3.5 V from the $I_{ds}-V_g$ curve.

The p-type conductivity of the ZnTe:N NRs can be facilely tuned by controlling the N doping level. Figure 5 shows the electrical transfer characteristics of a single ZnTe:N with 20% NH_3 during growth. The conductance of the ZnTe:N NR has dramatically increased as compared with the i-ZnTe and ZnTe:N NRs doping with 10% NH_3. The resistance and resistivity of
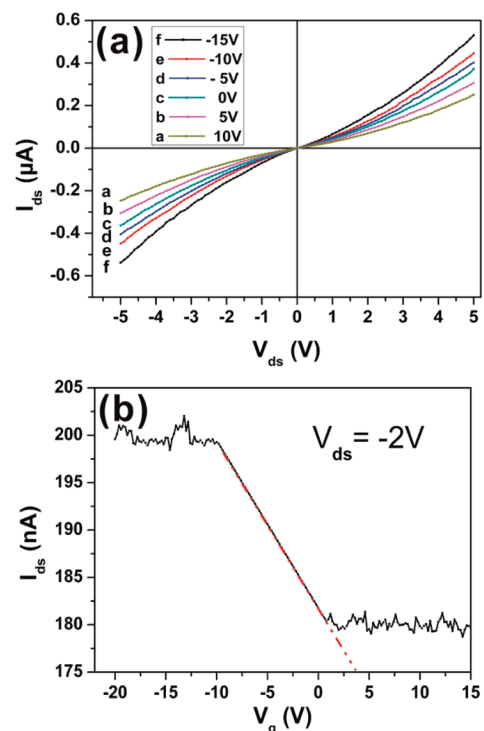
Figure 4. Electron-transfer characteristics of N-doped ZnTe SNRFET in N_2-NH_3 (90% + 10%) ambient. (a) I_{ds} vs V_{ds} curves for different V_g that range from 10 to (-15) V. (b) I_{ds} vs V_g curve measured at $V_{ds} = -2$ V.

the ZnTe:N NRs can be estimated to be 1.1×10^6 Ω and 0.14 Ω cm, respectively. The gate-dependent $I_{ds}-V_{ds}$ also reveals p-type conductivity. V_{th} and g_m can be estimated to be 4.0 V and 78.4 nS, respectively. In addition, taking into account the width (Z) of ZnTe of 230 nm and the channel length (L) of 4600 nm, the electron mobility (μ_h) of the device can be estimated to be about 1.2 cm^2 V^{-1} S^{-1}, and the hole concentration (p) can be approximately calculated to be 3.6×10^{19} cm^{-3}.

Further experiments had been carried out to synthesize p-ZnTe NR at different NH_3 concentrations ranging from 20%

7984 *J. Phys. Chem. C, Vol. 114, No. 17, 2010*

Li et al.
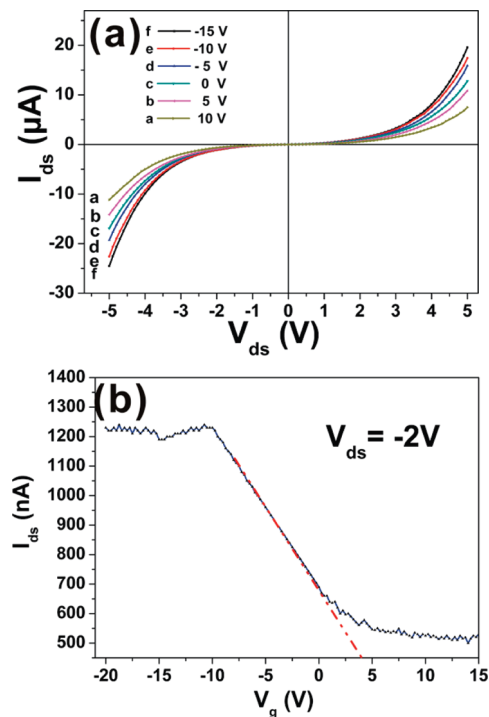
Figure 5. Electron-transfer characteristics of N-doped ZnTe SNRFET in N_2-NH_3 (80% + 20%) ambient. (a) I_{ds} vs V_{ds} curves for different V_g that range from 10 to (−15) V. (b) I_{ds} vs V_g curve measured at V_{ds} = −2 V.

to 50%, and the corresponding electrical measurements were also performed. Interestingly, the results reveal that the p-type conductivity of the ZnTe NRs synthesized at different NH_3 concentrations, ranging from 20% to 50%, remains unchanged obviously.

Electrical measurements demonstrated that N-doping led to a substantial enhancement in p-type conductivity of ZnTe NRs. Compared with the intrinsic counterpart, the electrical transport properties of the preceding doped ZnTe NRs exhibit a significant change. The carrier mobility (μ_h) increased from 6.2×10^{-3} $cm^2 V^{-1} S^{-1}$ to $1.2 cm^2 V^{-1} S^{-1}$, and the resistivity (ρ) declined from 45.1 Ω cm to 0.14 Ω cm. However, the hole concentration first declined from $2.2 \times 10^{19} cm^{-3}$ to $8.3 \times 10^{18} cm^{-3}$ and then increased to $3.6 \times 10^{19} cm^{-3}$. In comparison with the reported results,[19,29] the carrier mobility of ZnTe:N SNRFET greatly improved, while the resistivity (ρ) declined evidently.

The difference in p-type conductivity between i-ZnTe and ZnTe:N NRs can be understood in terms of fundamental principle of chemical reactions. For the i-ZnTe NRs, the inherent p-type conductivity mainly results from the component defect, namely, the Zn vacancy. On the other hand, the enhanced p-type conductivity of ZnTe:N can be mainly ascribed to the impurity defects owing to doping nitrogen atoms. In the case of the i-ZnTe NRs synthesized in $Ar-H_2$ ambient, as discussed above, the existing large numbers of Zn vacancies contribute to the high p-type carrier concentration. However, the resulting crystal defect will lead to high resistivity and low carrier mobility. In contrast, in the case of the ZnTe:N NRs synthesized in N_2-NH_3 ambient, the enhanced p-type conductivity can be ascribed to the doped N atoms substituting Te atoms. During the doping reaction process, the NH_3 molecules can decompose into N atoms and H atoms. Here, it is believed that NH_3 atmosphere acts as reducing ambient and N atoms serve as acceptor dopant. The doped N atoms will substitute for Te atoms in the crystal lattice and will form the so-called substitutional doping. In the

viewpoint of the electronegativity and the atomic radius, the electronegativity values of N and Te are 3.06 and 2.16,[42,43] and the atomic radius of N and Te are 0.075 and 0.142 nm, respectively. The higher electronegativity and the smaller atomic radius enable N atoms a stronger affinity to Zn atoms, which will consequently decrease the quantity of Zn vacancies during the crystal growth in view of the dynamics. As a result, the composition deviation from stoichiometry will decline. At a NH_3 concentration level of 10%, both the component defects and the composition deviation from stoichiometry will decline to a certain degree. The impurity defects will increase to some extent, which will in turn lead to the decrease in both the carrier concentration and the resistivity (ρ) and to an increase in the carrier mobility (μ_h). As the NH_3 concentration increased gradually, the effect of substitution doping increases accordingly. When the NH_3 concentration added up to 20%, the effect of substitution doping increases and plays a predominant role in the p-type transport properties. With the increasing NH_3 concentration, the Zn vacancies decrease gradually to a minimum value and the composition deviation from stoichiometry will decline to a minimum value. In other words, the ratio of Zn atoms to the rest of the atoms (including N and Te atoms) is close to stoichiometry. Meanwhile, the substitution doping reversely increases to a maximum value. As a result, under the combined action of the component defects and the impurity defects, the carrier concentration and the carrier mobility (μ_h) would increase and the resistivity (ρ) would decline. However, all the properties including the resistivity, the carrier concentration, and the carrier mobility remain unchanged when the NH_3 concentration exceeds 20% according to the further experiments of 20−50% NH_3 concentrations. In fact, for single-crystalline ZnTe NRs, the dopant concentration of N element is limited because of the compensation effect.[11,12,18] In our experiments, when the NH_3 concentration increases up to 20%, the N-doped effect can be found to be close to the limitation and the carrier concentration might reach the maximum value. All the electrical measurements based on both intrinsic and different N-doped degree ZnTe NRs demonstrated that N-doping led to a substantial enhancement in p-type conductivity of ZnTe NRs. Consequently, it is reasonable to conclude that the p-type conductivity of ZnTe NRs could be well adjusted by controlling NH_3 concentration in a wide range.

Conclusion

In summary, we have succeeded in preparing the i-ZnTe and ZnTe:N NRs via a simple thermal evaporation method. The i-ZnTe NRs show poor electrical transport properties because of plentiful crystal defects. In contrast, controllable N-doped method can effectively improve p-type conductivities yielding a resistivity of 1.4×10^{-1} Ω cm, a carrier concentration of $3.6 \times 10^{19} cm^{-3}$, and a mobility of $1.2 cm^2 V^{-1} S^{-1}$. X-ray photoelectron spectroscopy (XPS) studies semiquantitatively confirm N-doped concentration close to 1%. It is strongly believed that the as-prepared p-type ZnTe NRs with excellent electrical properties are promising building blocks for the future nanodevices, such as field-effect nanotransistors, electro-optic detectors, and solar cells.

Enhanced p-Type Conductivity of ZnTe Nanoribbons

J. Phys. Chem. C, Vol. 114, No. 17, 2010 **7985**

References and Notes

(1) Jiang, Y.; Zhang, W. J.; Jie, J. S.; Meng, X. M.; Fan, X.; Lee, S. T. *Adv. Funct. Mater.* **2007**, *17* (11), 1795–1800.

(2) Jie, J. S.; Zhang, W. J.; Jiang, Y.; Meng, X. M.; Li, Y. Q.; Lee, S. T. *Nano Lett.* **2006**, *6* (9), 1887–1892.

(3) Jiang, Y.; Meng, X. M.; Liu, J.; Hong, Z. R.; Lee, C. S.; Lee, S. T. *Adv. Mater.* **2003**, *15* (14), 1195–1198.

(4) Pan, Z. W.; Dai, Z. R.; Wang, Z. L. *Science* **2001**, *291* (5510), 1947–1949.

(5) Wang, Z. L.; Song, J. H. *Science* **2006**, *312* (5771), 242–246.

(6) Janik, E.; Dluzewski, P.; Kret, S.; Presz, A.; Kirmse, H.; Neumann, W.; Zaleszczyk, W.; Baczewski, L. T.; Petroutchik, A.; Dynowska, E.; Sadowski, J.; Caliebe, W.; Karczewski, G.; Wojtowicz, T. Catalytic growth of ZnTe nanowires by molecular beam epitaxy: structural studies. *Nanotechnology* **2007**, *18*, 475606.

(7) Jie, J. S.; Zhang, W. J.; Jiang, Y.; Meng, X. M.; Zapien, J. A.; Shao, M. W.; Lee, S. T. *Nanotechnology* **2006**, *17* (12), 2913–2917.

(8) Jie, J. S.; Zhang, W. J.; Jiang, Y.; Lee, S. T. *App. Phys. Let.* **2006**, *89* (22), 223117.

(9) Wang, Z. L. *Acs Nano* **2008**, *2* (10), 1987–1992.

(10) Zappettini, A.; Spano, N.; Mazzera, M.; Guadalupi, G. M.; Paorici, C. *J. Cryst. Growth* **2008**, *310* (7−9), 2080–2084.

(11) Tianling Ren, J. Z. *Comput. Appl.Chem.* **1998**, *15* (6), 327–332.

(12) Zumbiehl, A.; Mergui, S.; Ayoub, M.; Hage-Ali, M.; Zerrai, A.; Cherkaoui, K.; Marrakchi, G.; Darici, Y. *Mater. Sci. Eng., B* **2000**, *71* (1−3), 297–300.

(13) Wang, Z. L. *Mater. Sci. Eng., R* **2009**, *64* (3−4), 33–71.

(14) Majumdar, S.; Chattopadhyay, S.; Banerji, P. *Appl. Surf. Sci.* **2009**, *255* (12), 6141–6144.

(15) Yuan, G. D.; Zhang, W. J.; Jie, J. S.; Fan, X.; Zapien, J. A.; Leung, Y. H.; Luo, L. B.; Wang, P. F.; Lee, C. S.; Lee, S. T. *Nano Lett.* **2008**, *8* (8), 2591–2597.

(16) Yuan, G. D.; Zhang, W. J.; Zhang, W. F.; Fan, X.; Bello, I.; Lee, C. S.; Lee, S. T. *Appl. Phys. Lett.* **2008**, *93* (21), 213102.

(17) Song, H. S.; Zhang, W. J.; Yuan, G. D.; He, Z. B.; Zhang, W. F.; Tang, Y. B.; Luo, L. B.; Lee, C. S.; Bello, I.; Lee, S. T. *Appl. Phys. Lett.* **2009**, *95* (3), 033117.

(18) Adachi, S. *Properties of Group-IV, III-V and II-VI Semiconductors*; Wiley Press: West Sussex, U.K., 2005; pp 127, 339.

(19) Zhang, J.; Chen, P. C.; Shen, G. Z.; He, J. B.; Kumbhar, A.; Zhou, C. W.; Fang, J. Y. *Angew. Chem., Int. Ed.* **2008**, *47* (49), 9469–9471.

(20) Lieber, C. M.; Wang, Z. L. *MRS Bull.* **2007**, *32* (2), 99–108.

(21) Meng, Q. F.; Jiang, C. B.; Mao, S. X. *Appl. Phys. Let.* **2009**, *94* (4), 043111.

(22) Sato, K. T. A.; Hanafusa, M.; Noda, A.; Arakawa, A.; Uchida, M.; Oda, O.; Yamada, Y.; Taguchi, T. *Phys. Status Solidi A* **2000**, *180* (1), 267–274.

(23) Tit, N. *J. Vac. Sci. Technol., A* **2004**, *22* (3), 821–825.

(24) Kröger, F. A. *J. Phys. Chem.* **1965**, *69* (10), 3367–3369.

(25) John, V. S.; Mahalingam, T.; Chu, J. P. *Solid State Electron.* **2005**, *49* (1), 3–7.

(26) Li, L.; Yang, Y. W.; Huang, X. H.; Li, G. H.; Zhang, L. D. *J. Phys. Chem. B* **2005**, *109* (25), 12394–12398.

(27) Yong, K. T.; Sahoo, Y.; Zeng, H.; Swihart, M. T.; Minter, J. R.; Prasad, P. N. *Chem. Mater.* **2007**, 4108–4110.

(28) Colli, A.; Fasoli, A.; Hofmann, S.; Ducati, C.; Robertson, J.; Ferrari, A. C. *Nanotechnology* **2006**, *17* (4), 1046–1051.

(29) Huo, H. B.; Dai, L.; Liu, C.; You, L. P.; Yang, W. Q.; Ma, R. M.; Ran, G. Z.; Qin, G. G. *Nanotechnology* **2006**, *17* (24), 5912–5915.

(30) Yamamoto, T. *Jpn. J. Appl. Phys. 2* **2003**, *42* (5B), L514–L516.

(31) Cao, P.; Zhao, D. X.; Zhang, J. Y.; Shen, D. Z.; Lu, Y. M.; Yao, B.; Li, B. H.; Bai, Y.; Fan, X. W. *Appl. Surf. Sci.* **2008**, *254* (9), 2900–2904.

(32) Baron, T.; Tatarenko, S.; Saminadayar, K.; Magnea, N.; Fontenille, J. *Appl. Phys. Lett.* **1994**, *65* (10), 1284–1286.

(33) Tamargo, M. C. *II-VI Semiconductor Materials and their Applications*, 1st ed.; Optoelectronic Properties of Semiconductors and Superlattices, Vol. 12; CRC Press: New York, 2002; p 92.

(34) Meng, Q. F.; Jiang, C. B.; Mao, S. X. *J. Cryst. Growth* **2008**, *310* (20), 4481–4486.

(35) Huo, H. B.; Dai, L.; Xia, D. Y.; Ran, G. Z.; You, L. P.; Zhang, B. R.; Qin, G. G. *J. Nanosci. Nanotechnol.* **2006**, *6* (4), 1182–1184.

(36) Sze, S. M.; Ng, K. K. *Physics of Semiconductor Devices*, 3rd ed; Wiley Press: New Jersey, 1981; Chapter 8.2, p 456.

(37) Javey, A.; Kim, H.; Brink, M.; Wang, Q.; Ural, A.; Guo, J.; McIntyre, P.; McEuen, P.; Lundstrom, M.; Dai, H. J. *Nat. Mater.* **2002**, *1* (4), 241–246.

(38) Bhattacharyya, D.; Chaudhuri, S.; Pal, A. K. *Mater. Chem. Phys.* **1995**, *40* (1), 44–49.

(39) Bensahel, D.; Dupuy, M.; Pfister, J. C. *J. Cryst. Growth* **1979**, *47* (5−6), 727–732.

(40) Wang, W. W.; Xia, G. P.; Zheng, J. G.; Feng, L. H.; Hao, R. Y. *J. Mater. Sci. Mater. Electron.* **2007**, *18* (4), 427–431.

(41) Murali, K. R.; Rajkumar, P. R. *J. Mater. Sci. Mater. Electron.* **2006**, *17* (5), 393–396.

(42) Mann, J. B.; Meek, T. L.; Allen, L. C. *J. Am. Chem. Soc.* **2000**, *122* (12), 2780–2783.

(43) Mann, J. B.; Meek, T. L.; Knight, E. T.; Capitani, J. F.; Allen, L. C. Configuration Energies of the d-Block Elements. *J. Am. Chem. Soc.* **2000**, *122* (21), 5132–5137.

JP911873J